Enhanced Chemical Classification of Raman Images Using Multiresolution Wavelet Transformation

T. TONY CAI, DONGMAO ZHANG, and DOR BEN–AMOTZ*

Department of Statistics, The Wharton School, University of Pennsylvania, Philadelphia, Pennsylvania 19104 (T.T.C.); and Department of Chemistry, Purdue University, West Lafayette, Indiana 47907-1393 (D.Z., D.B.-A.)

Multiresolution wavelet transformation (MWT) and block thresholding is used to effectively suppress both background and noise interference while minimally distorting Raman spectral features. The performance of MWT as a spectral pre-processing algorithm is demonstrated using both synthetic spectra and experimental hyper-spectral Raman images with large background and noise components. The results are quantified by comparing correlation coefficients of synthetic spectra with either the same or different backgrounds. The improved chemical imaging performance obtained using MWT is demonstrated by comparing principal component analysis (PCA) channel images and spectral angle mapping (SAM) classified images before and after MWT pre-processing.

Index Headings: **Raman imaging; Wavelet transform; Image classification; Denoise; Block threshold.**

INTRODUCTION

The utility of Raman microscopy in chemical imaging of biological, organic, and inorganic materials is increasingly becoming recognized.[1–3] The power of this method derives from the high chemical information content of Raman spectra, while the most significant obstacle to its widespread application often results from interfering noise and background (fluorescence) signals. This work reports the application of a multiresolution wavelet transformation (MWT) signal processing algorithm to efficiently separate noise and background signals from Raman spectral features, for enhanced chemical classification and imaging.

Previous methods used to eliminate fluorescence background include Spline fit subtraction (SFS),[4] fast-Fourier transformation (FFT) high-pass and low-pass filtering,[5] and Savitzky–Golay (SG) smoothing and derivation extraction[6,7] algorithms. Although each of these have proven to be quite useful, they also have significant limitations. The SFS method often requires sample dependent optimization in defining background regions. The FFT method typically attenuates and distorts Raman spectral features unless these are well separated from the Fourier frequency components of the background and noise. The SG based methods, although recently shown to be quite useful for fluorescence and noise suppression,[6] also inevitably distort Raman spectral features. The MWT method presented in this work is found to preserve Raman spectral integrity while selectively rejecting noise and background components. Thus, the MWT method appears to have many of the advantages with fewer of the drawbacks of previously proposed Raman spectral preprocessing methods.

Received 2 February 2001; accepted 14 May 2001.
* Author to whom correspondence should be sent.

Wavelet transformation (WT) is a rapidly evolving branch of applied mathematics that is increasingly recognized for its relevance to analytical chemistry.[8] Unlike FFT, which uses sinusoidal functions as basis sets, WT uses localized wavelet functions that better represent spectral bands, background, and noise features typically encountered in spectroscopic data. Previous applications of WT methods have demonstrated its utility in spectral data compression,[9] removal of baseline drift and noise,[10,11] chemical classification,[12] and regression using wavelet coefficients.[13] However, no previous studies have applied WT to Raman image processing. Achieving this goal requires a robust WT algorithm that can simultaneously process large numbers of spectra each containing significant variations in signal, noise, and background intensity and shape.

Wavelet methods have demonstrated considerable success in statistical function estimation in terms of spatial adaptivity, computational efficiency, and asymptotic optimality. Wavelets are known for their excellent compression and localization properties. In many cases of interest, information about a signal is largely contained in a relatively small number of large coefficients. Standard wavelet methods achieve adaptivity through term-by-term thresholding of the empirical wavelet coefficients. Donoho and Johnstone's VisuShrink[18] is a well-known example. It has been shown that one can further increase estimation precision by utilizing information about neighboring wavelet coefficients. A block thresholding procedure, proposed by Cai,[19] thresholds the empirical wavelet coefficients in groups rather than individually. The procedure makes simultaneous decisions to retain or to discard all the coefficients within a block. The estimator enjoys a higher degree of adaptivity than the standard term-by-term thresholding methods. The improvement in estimation accuracy can be quite significant.

In this paper, we extend the block thresholding method for function estimation to chemical classification and imaging. We demonstrate the use of MWT and block thresholding in suppressing both fluorescence background and noise interference, while minimally attenuating or distorting the Raman spectral features of interest. After describing the theoretical basis of the method, its performance is tested using both synthetic and experimental Raman spectral data. Synthesized data sets are used to quantify the separation of noise, background, and spectral features. Experimental application of MWT is demonstrated using Raman imaging data collected from microscopic samples of commercial drugs, on a substrate producing a strongly wavelength dependent background interference. Chemical classification of the resulting images

0003-7028/01/5509-1124$2.00/0

is achieved by combining MWT pre-processing with principal component analysis (PCA) and spectral angle mapping (SAM) post-processing algorithms.[2,14]

WAVELET PREPROCESSING

The approach we take in implementing MWT is to first identify and remove the smooth background, then remove the random noise contamination, and finally chemically classify the material by measuring the distance between the processed spectrum and standard library spectra. We begin by briefly outlining the MWT method, followed by separate discussions of the MWT background removal and noise removal procedures.

Wavelet bases are special orthonormal functions in L_2 space. They offer a degree of localization both in space and in frequency. Wavelet series provide a simpler and more efficient way to analyze signals that have been traditionally studied by means of Fourier series. Wavelets provide excellent compression and localization properties and thus promise to be very useful for Raman imaging applications, which may generate large data files containing relatively sharp (localized) spectral features.

A one-dimensional orthonormal wavelet basis is generated from dyadic dilation and integer translation of two basic functions, a ''father'' wavelet ϕ and a ''mother'' wavelet ψ. More specifically, let

$$\phi_{j,k}(x) = 2^{j/2}\phi(2^j x - k) \quad \text{and} \quad \psi_{j,k}(x) = 2^{j/2}\psi(2^j x - k)$$

with both j and k integers. The functions $\psi^{j,k}$ are obtained by first translating (or moving) the mother wavelet ψ along the line by k units and then squeezing the translated ψ by a factor of 2^j. The collection $\{\phi_{j0,k},\ 1 \le k \le 2^{j0}\} \cup \{\psi_{j,k},\ 1 \le k \le 2^j,\ j \ge j_0\}$ forms an orthonormal wavelet basis in which $\phi_{j0,k}$ captures the gross smooth structure of the signal, and the $\psi_{j,k}$ functions (with $j = j_0, j_0 + 1, \ldots$) represent progressively finer scale deviations from the smooth behavior.

Furthermore, the functions ϕ and ψ can be chosen to be compactly supported. That is, the functions are nonzero only within a finite interval and vanish everywhere outside the interval. An orthonormal wavelet basis generated from compactly supported wavelets has an associated exact orthogonal discrete wavelet transform that transforms a discrete signal into the wavelet coefficient domain in linear time, which is even faster than the FFT.

The MWT algorithm is a multiresolution decomposition WT procedure that decomposes a signal into orthogonal resolution components at different scales. The fine scale features are captured by the wavelet coefficients at fine resolution levels (and labeled D_i, where $i = 1, 2, 3, \ldots$). The smooth component is captured by the coefficients at the coarse level (and labeled S_i, where $i = 1, 2, 3, \ldots$). For more on wavelets and multiresolution analysis, the reader is referred to previous papers and books by Mallat, Daubechies, and Meyer.[15–17]

Background Removal Procedure. Figure 1 illustrates the use of the multiresolution decomposition procedure for background removal. Panel (**a**) shows a synthesized spectrum and a smooth broadband background. The background is a sinusoid and the signal consists of a sequence of sharp spikes that resembles actual Raman spectra observed in practice. The analytic formula for the signal is, as given in Ref. 18,

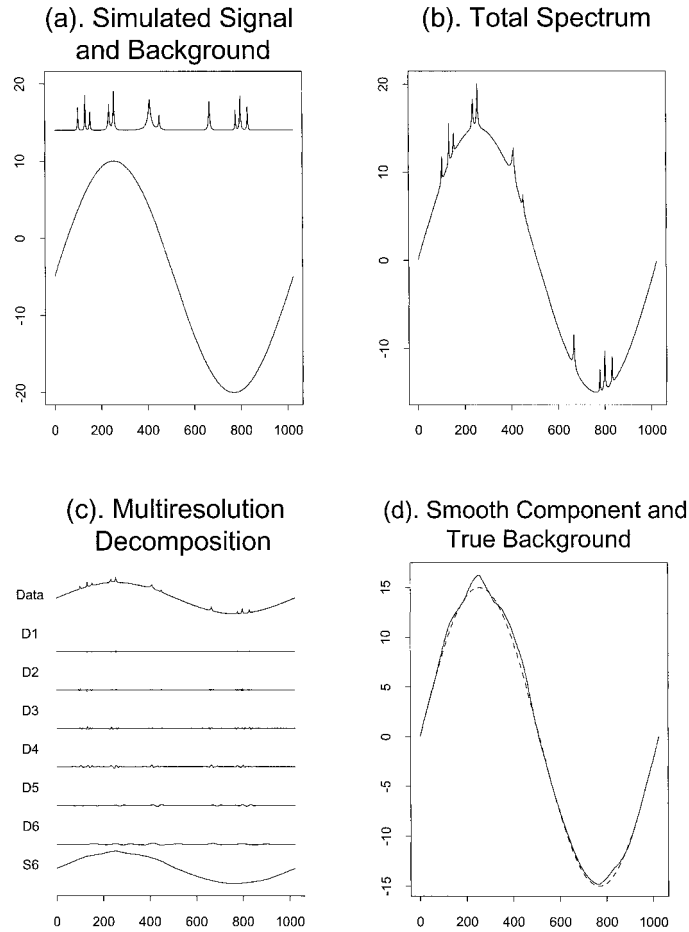

FIG. 1. Multiresolution decomposition feature of MWT is used to remove a slowly varying background from a simulated spectrum (see text for details).

$$f(x) = 15.0769 \cdot \sum h_j K((x - x_j)/w_j)$$

$$\text{with } K(x) = (1 + |x|)^{-4}$$

$$(x_j) = (.1, .13, .15, .23, .25, .40, .44, .65, .76, .78, .81)$$

$$(h_j) = (4, 5, 3, 4, 5, 4.2, 2.1, 4.3, 3.1, 5.1, 4.2)$$

$$(w_j) = (.005, .005, .006, .01, .01, .03, .01, .01, .005, .008, .005)$$

The simulated signal is the superposition of the two components, and the objective is to remove the broadband background. To do that, we decompose the total signal into different scale components (panel (**c**)). We then use the smooth component at the lowest resolution level (S_1) as our estimate of the broadband background (panel (**d**), solid line). It is smooth and comes very close to the true background (panel (**d**), dotted line). This procedure is automatic, as it does not assume any knowledge of the particular structure of the background except that it is smooth and of low frequency (slowly varying).

Furthermore, the above procedure is robust against random noise contamination. In Fig. 2 we add Gaussian

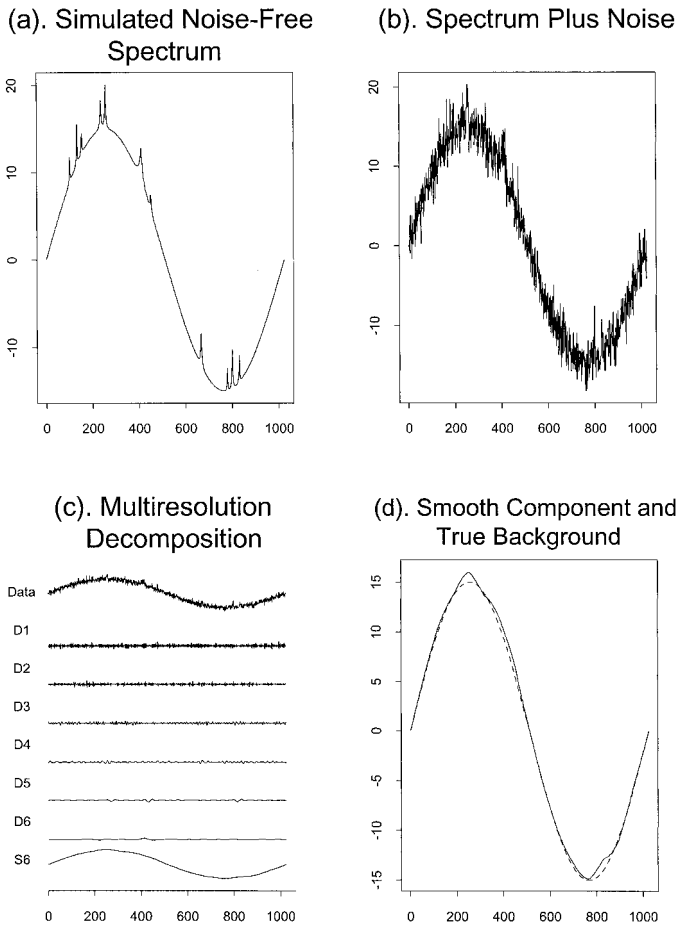

FIG. 2. The MWT background removal algorithm works equally well in the presence of noise (compare to Fig. 1).

noise to the signal and apply the same procedure to the simulated noisy spectra (panels (**b**) and (**c**)). The smooth component at the lowest resolution level is virtually unchanged (see panel (**d**)). This robustness clearly makes the MWT background removal procedure valuable for our problem.

Noise Removal Procedure. Wavelet methods have also demonstrated considerable success in nonparametric function estimation where one wishes to remove noise and recover the true signal based on noisy observations. In contrast to the traditional linear procedures, wavelet methods achieve (near) optimal performance over large function classes and enjoy excellent performance when used to estimate functions that are spatially inhomogeneous.

Wavelets are known for their excellent compression and localization properties. In many cases of interest, information about a function is essentially contained in a relatively small number of large coefficients. Standard wavelet methods achieve adaptivity through term-by-term thresholding of the empirical wavelet coefficients. There, each individual empirical wavelet coefficient is compared with a predetermined threshold. A wavelet coefficient is retained if its magnitude is above the threshold level and is discarded otherwise. A well-known example of term-by-term thresholding is Donoho and Johnstone's VisuShrink.[18]

Cai[19] has recently shown that one can increase estimation accuracy by utilizing information about neighboring wavelet coefficients. A block thresholding procedure, called BlockJS, proposed by Cai, thresholds the empirical wavelet coefficients in groups rather than individually. The procedure makes simultaneous decisions to retain or to discard all the coefficients within a block. As shown by Cai,[19] the block thresholding estimator simultaneously achieves three objectives: adaptivity, spatial adaptivity, and computational efficiency. The estimator enjoys a higher degree of adaptivity than the standard term-by-term thresholding methods. The BlockJS procedure can be described in three steps:

(1) Transform the data into the wavelet domain *via* the discrete wavelet transform.

(2) At each resolution level j, group the empirical wavelet coefficients ($\tilde{\theta}_{jk}$) into disjoint b_i^j of length $L = \log n$. Let $\lambda = 4.5053$ and $S_{ji}^2 = \Sigma_{(j,k)\in b_i^j} \tilde{\theta}_{j,k}^2$. Within each block b_i^j, estimate the coefficients simultaneously *via* a shrinkage rule

$$\tilde{\theta}_{j,k} = (1 - \lambda L\sigma^2/S_{ji}^2) + \tilde{\theta}_{j,k}, \quad \text{for all } (j, k) \in b_i^j \quad (1)$$

(3) Apply the inverse discrete wavelet transform to the denoised wavelet coefficients to yield the estimate of the function.

The block length $L = \log n$ and the thresholding constant $\lambda = 4.5053$ are chosen based on theoretical considerations. The BlockJS estimator enjoys excellent asymptotic and finite-sample performance.

In Eq. 1 the quantity σ is the noise level that is estimated as the median absolute deviation of the wavelet coefficients at the finest level divided by 0.6745. For further details, see Cai[19] as well as Donoho and Johnstone.[18]

Figure 3 shows an example of BlockJS in action. The simulated noisy signal is shown in panel (**a**). We first apply the wavelet transform to the noisy signal and the empirical wavelet coefficients are displayed in panel (**b**). The coefficients are organized in the natural multiresolution style. The block shrinkage rule (Eq. 1) is applied to the empirical coefficients and the resulting estimate of the true wavelet coefficients are displayed in panel (**c**). The inverse wavelet transform of the estimated wavelet coefficients is the estimate of the true signal and is shown in panel (**d**) (solid line). The dotted line in panel (**d**) is the true signal. It is clear that the BlockJS estimator captures both the smooth and the peaked features of the true signal well.

Chemical Classification Procedure. In Raman chemical classification and imaging, the observed signals are typically contaminated by both random noise and smooth broadband background components. The random noise contamination in Raman spectra is typically heteroscedastic. In other words, the noise varies from wavelength to wavelength and typically has a variance equal to the mean signal at each wavelength. This creates additional difficulties because standard noise removal procedures are mainly restricted to homoscedastic (wavelength independent) noise. Furthermore, in Raman spectroscopic applications the fluorescence background is often larger than the true Raman spectral features. Therefore we can use the fluorescence background spectra as good estimates of the variances of the random noise and use this

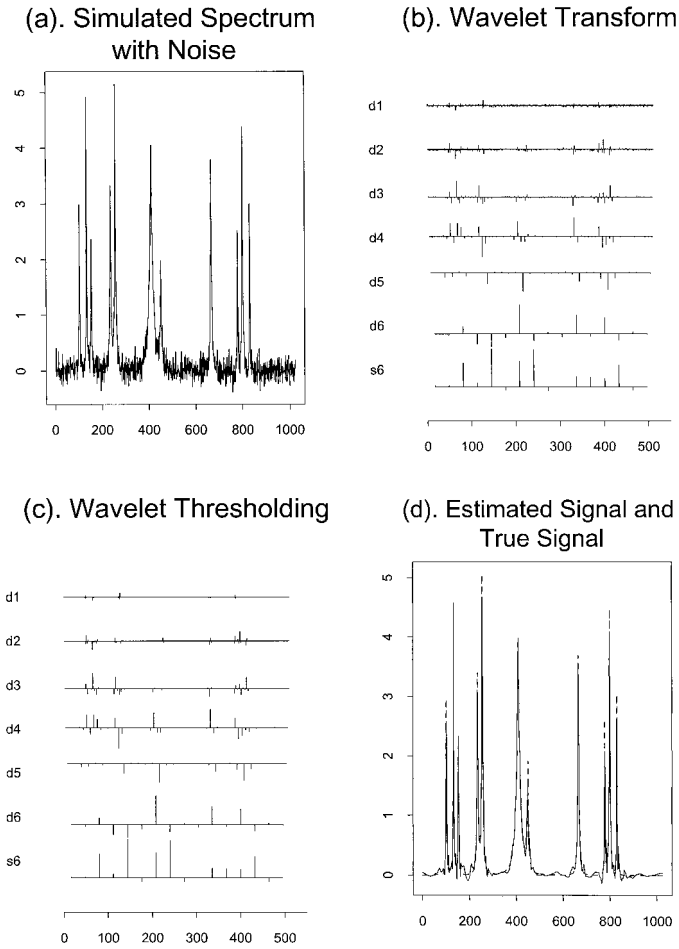

FIG. 3. Wavelet thresholding MWT is used to remove noise from a simulated spectrum (see text for details).

information to renormalize the signal and make the noise more nearly homoscedastic.

The following three steps summarize the procedure we use to implement multiresolution analysis and block thresholding for chemical classification of Raman images.

(1) Use the multiresolution decomposition procedure to remove background by separating the observed Raman spectra into two components. The first component is the estimated smooth broadband background and the second is the difference between the observed spectra and the estimated background spectra, which is assumed to be the "true" Raman spectrum contaminated with random noise.
(2) Normalize the second component by dividing *it* by the square root of the estimated background spectra. The random noise in the normalized signal is now nearly homoscedastic. Apply the BlockJS procedure to remove the random noise. Then renormalize the estimated signal by multiplying it by the square root of the estimated background spectra to obtain the final processed spectra.
(3) Chemically classify the spectrum by measuring its distance from a set of standard library spectra (e.g., using the SAM algorithm).

Synthesized Spectral Analysis. The class separability improvement achievable using the MWT method is demonstrated with a set of six synthesized spectra shown in Fig. 4. These are the same synthetic spectra that have previously been used by Zhang and Ben–Amotz in demonstrating the performance of the SG second derivative (SGSD) pre-processing algorithm.[6] Since SGSD was found to be a very effective method for suppressing noise and fluorescence interference and enhancing the chemical classification of Raman images, the present comparison is a valuable test of the MWT method. These synthetic spectra have been generated by combining three different model Raman spectra A, B, and C with two model backgrounds 1 and 2, as described previously.[6] The input spectra are shown in the upper six panels of Fig. 4 and resulting MWT pre-processed output spectra are shown in the lower six panels of Fig. 4.

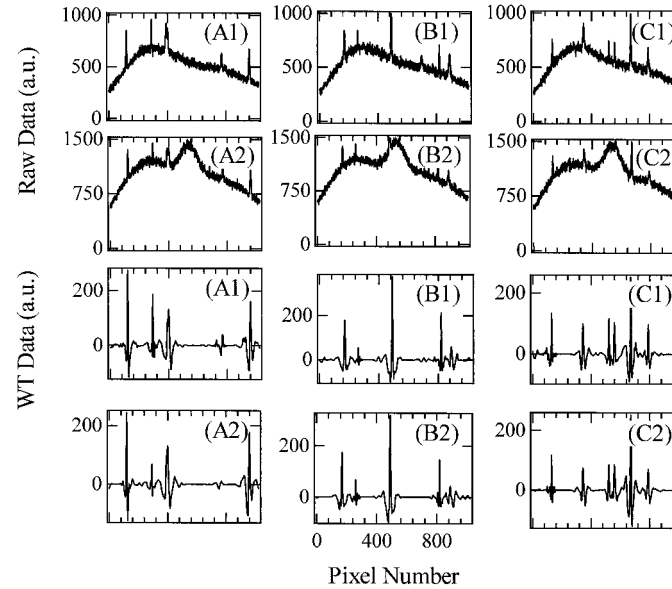

FIG. 4. Simulated Raman spectra with Gaussian spectral and background features and Poisson noise. Spectra A1, B1, and C1 contain three different Raman spectra (A, B, C) with the same fluorescence background (1), while A2, B2, and C2 contain the same three Raman spectra with a different fluorescence background (2).

For a successful classification, spectra A1 and A2, B1 and B2, and C1 and C2 should be classified into three distinct groups based on their similarity. The similarity between two spectra is measured by their correlation coefficient, with a larger correlation coefficient (near 1) indicating stronger similarity. The bar graph in Fig. 5 shows the correlation coefficients obtained among nine spectral pairs before (Fig. 5a) and after (Fig. 5b) MWT

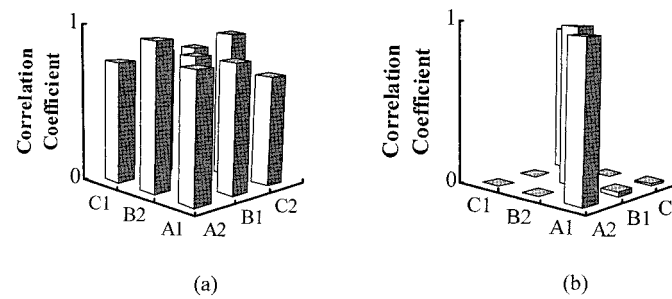

FIG. 5. Correlation coefficients between the spectra shown in Fig. 4 before (**a**) and after (**b**) the MWT pre-processing.

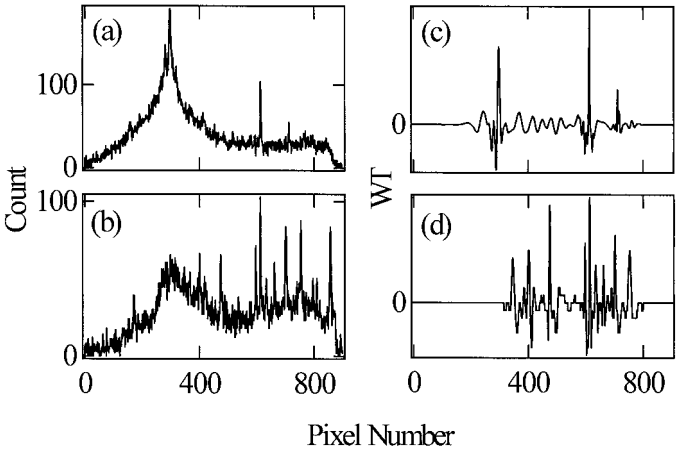

FIG. 6. Representative Raman spectra obtained from a single image pixel containing Aleve (upper) or Bayer (lower) on a glass substrate with large broadband background interference. The left frames contain raw spectra, and the right frames contain the corresponding MWT pre-processed spectra.

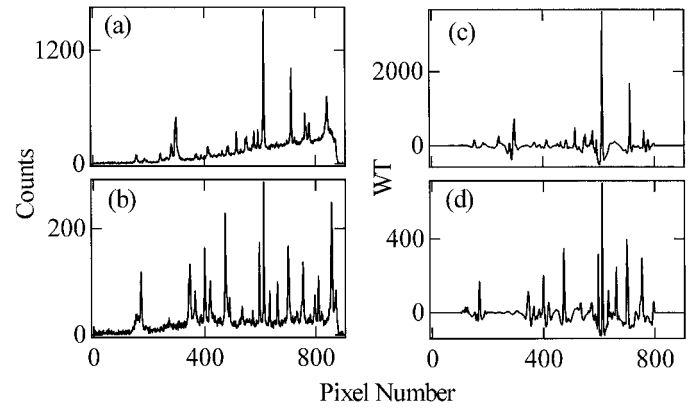

FIG. 7. Training spectra of Aleve and Bayer collected from a thick layer of sample (with no substrate interference). The left frames contain raw Raman spectra, and the right frames contain the corresponding MWT pre-processed Raman spectra.

pre-processing. Ideally, the bars in the diagonal positions should be close to 1 (indicating strong spectral similarity) while the off diagonal bars should be small (indicating insensitivity to background features).

The results obtained before MWT pre-processing (Fig. 5a) show that the spectra with the same background have very high correlation coefficients regardless of whether the Raman features contained in these spectra are the same or not. In other words, the large backgrounds overshadow the Raman spectral features.

The background correlation is efficiently eliminated after the MWT processing as demonstrated by the results shown in Fig. 5b. The maximum off diagonal correlation coefficient is 0.03, while the minimum diagonal element is 0.94. These results are better than those previously obtained using the SGSD method, in which the minimum diagonal (Raman spectral) correlation coefficient was 0.89,[6] and thus demonstrate the improved background suppression and denoising of the MWT pre-processing algorithm.

Raman Image Data Collection and Processing. Raman images of commercial medications, Aleve (naproxen) and Bayer (aspirin), were collected with a near-IR Raman imaging microscope (NIRIM).[2,20] A single-frame spectral image collected by the NIRIM consists of an 8 $\times$ 10 rectangle array of Raman spectra, each with 900 wavelength channels (spanning a 75 to 1850 cm^{-1} Raman shift window). The single frame field of view of 55 μm $\times$ 44 μm is obtained when a 20$\times$ microscope objective (Olympus IC-20) is used. All spectra were collected with an integration time of 100 s. The sampled region was globally illuminated with a 785 nm diode laser (SDL-8360), and laser power reaching the active sample area was about 80 mW (about 1 mW per image pixel).

After scratching off the coating on the surface of the medication tablets, the powered medication was placed on one of the two different substrates: (1) a 0.9 mm thick glass microscope slide with a large broadband background emission or (2) a 22 $\times$ 50 mm quartz microscope slide (Ted Pella Inc.) with low background emission. The sample thickness was adjusted so as to produce relatively high substrate background interference.

Representative individual Raman spectra collected from two single image pixels containing Aleve (**a**) and Bayer (**b**), respectively, are shown in Fig. 6. The left two spectra are the raw data, and the right pair represent the same spectra after MWT pre-processing. The first and last 100 data points in the processed spectra are truncated to eliminate edge distortion produced by the MWT algorithm.

Training spectra were acquired in order to implement the SAM parametric classification method for chemical identification.[2,14] The conditions used to collect the training spectra are identical to those used to collect Raman images except for the longer integration time (300 s) and thicker sample layer (about 1.5 mm). The left pair of spectra shown in Fig. 7 are raw training spectra, and the right pair are the same spectra after MWT processing. Again, spectrum (**a**) is Aleve and (**b**) is Bayer. The background training spectra (not shown) are acquired with no sample and no substrate. These training spectra represent regions in which no sample is present, while avoiding bias introduced by background spectra from some specific substrate.

After the four different single frame images were acquired from two samples on two substrates, the four images were combined into a spectral data cube for processing and analysis. Image classification was performed using the MultiSpec software package.[14] This software allows the creation of single or multiple channel chemical images using either parametric methods such as the SAM quadratic classifier, nonparametric methods such as PCA, or combined methods including feature selection.

Figure 8 shows the PCA score images obtained from the same data set after spectral normalization, i.e., each spectrum vector in the data set is scaled to the same norm. The first column in the figure is the bright field image; the upper two are Aleve on glass slide and quartz slide while the lower two are Bayer on glass slide and quartz slide. The numbers shown above each column indicate the PCA channel from which the score for each spectrum is generated. Without the spectral normalization, the PCA score images contain little chemical information (not shown) because the spectral intensity fluc-

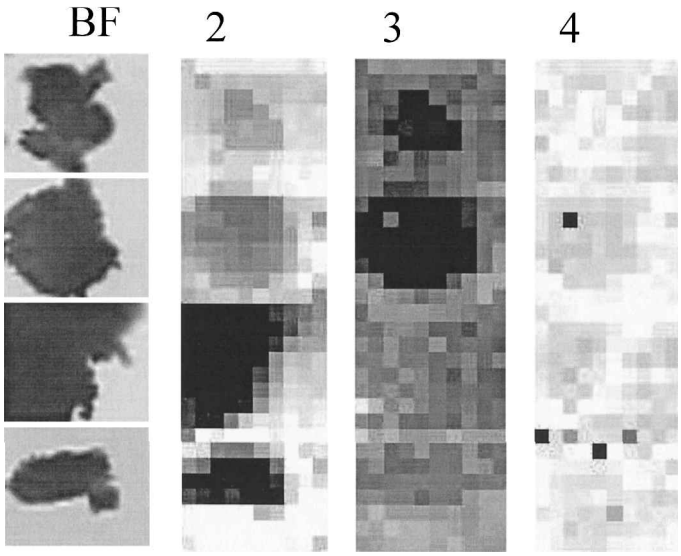

FIG. 8. Bright field (BF) and PCA channel images obtained after normalization of the image pixel spectra. Two distinct chemical components, Aleve (upper two rows) and Bayer (lower two rows), are evident in the second and third PCA channel images (see text for details).

tuation causes large channel score variation. Note that the score images for the first PCA channel are not shown because this PCA channel is in all cases dominated by background and noise. Figure 8 clearly reveals the different chemical identities of the two medications (with Bayer represented best by PCA channel 2 and Aleve by PCA channel 3).

Because of the improved performance obtained when using normalized spectra rather than raw data, all of the subsequent MWT pre-processed spectra were normalized prior to PCA analysis. Figure 9 shows the PCA channel image after MWT processing. The image quality is improved and the background is greatly reduced in both cases. There is so little background after MWT pre-processing that the first two channel score images in this case contain almost all of the chemical component information. Comparison of Figs. 8 and 9 reveals the improved image quality (sharper sample boundaries and greater contract) achieved after MWT pre-processing.

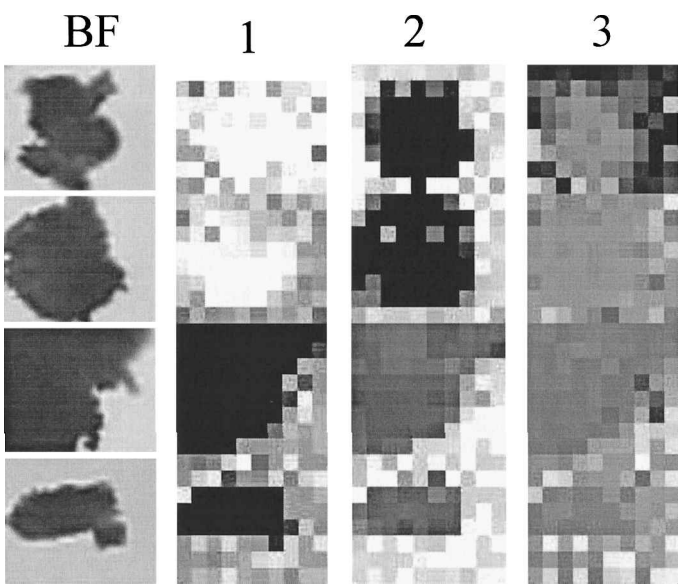

FIG. 9. Bright field (BF) and PCA channel images obtained after MWT pre-processing and normalization of the image pixel spectra. Two chemical components are clearly shown in the first two PCA channel images (see text for details).

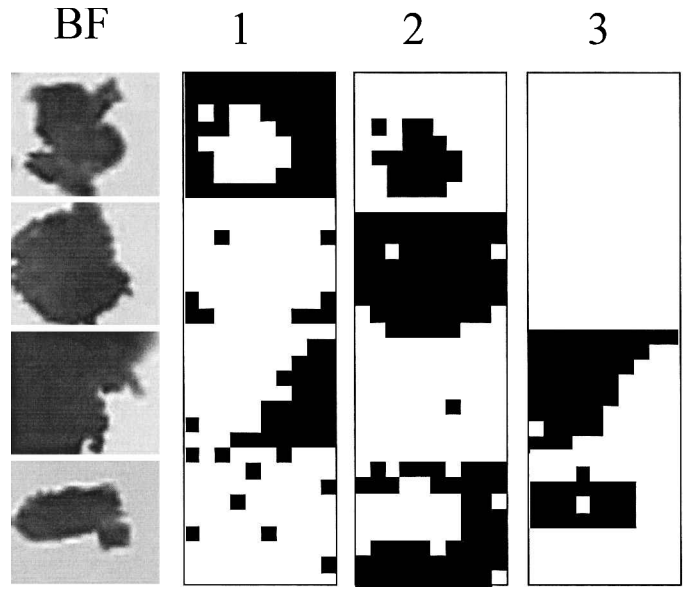

FIG. 10. Bright field (BF) and SAM channel images obtained with raw image spectra. Channels 1, 2, and 3 should represent background, Aleve, and Bayer, respectively, but chemical information content is largely obscured by the strong fluorescence background.

Figures 10 and 11 show the classified raw data image obtained using SAM before (Fig. 10) and after (Fig. 11) MWT pre-processing. The SAM algorithm compares the spectrum vector angle with that of the training spectrum vector. If the angles are within a pre-set cut-off then the corresponding image pixel is classified (colored black) as

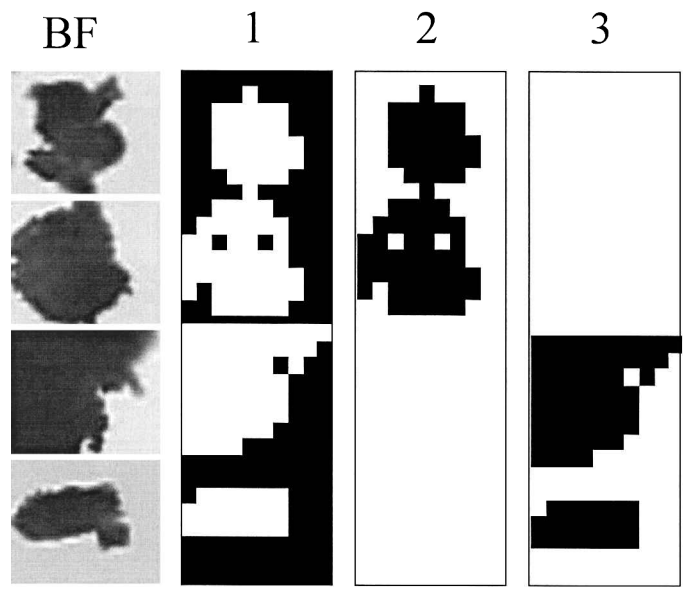

FIG. 11. Bright field (BF) and SAM channel images obtained with MWT pre-processed image spectra illustrating the effective components of the corresponding spectral images. Channels 1, 2, and 3 representing background, Aleve, and Bayer, respectively, are clearly segregated into mutually exclusive classes.

the corresponding component. Channels 1, 2, and 3 represent regions classified as background, Aleve, and Bayer components, respectively. The greatly improved performance SAM classification obtained after MWT pre-processing is even more clearly evident than in the PCA images. In particular, the images in Fig. 10 are only weakly correlated with the locations of the medication samples, while those in Fig. 11 very closely track the locations of the substrate and two medications.

SUMMARY AND DISCUSSION

It is evident that MWT processing can effectively suppress background and noise interference in Raman spectral classification applications. The background suppression capability of MWT may be viewed as an adaptive background curve fitting method that does not require specification of background and signal containing regions. Thus, MWT background subtraction may prove to be useful for automated processing of large spectral data sets and spectral images.

The computation time associated with MWT pre-processing is not a significant obstacle, since this algorithm is equivalent to digital curve convolution. Although the time required to perform an MWT is about 10 times more than that required for SGSD pre-processing, MWT has better noise suppression and introduces much lower spectral distortion.

Further applications of MWT in Raman imaging include classification in the wavelet domain by using the MWT coefficients as data channels. Such an approach could significantly improve classification speed and reduce the memory required to store large hyperspectral Raman data cubes. Thus, MWT shows significant promise in large scale spectral data analysis, molecular identification, and chemical imaging applications.

1. N. J. Kline and P. J. Treado, J. Raman Spectrosc. **28,** 119 (1997).
2. B. L. McClain, H. G. Hedderich, A. D. Gift, D. Zhang, K. N. Jallad, K. S. Haber, J. Ma, and D. Ben–Amotz, Spectrosc. **15,** 28 (2000).
3. M. D. Morris, J. A. Timlin, A. Carden, C. P. Tarnowski, and C. M. Edwards, Proc. SPIE-Int. Soc. Opt. Eng. **3920,** 151 (2000).
4. C. M. Stellman, K. S. Booksh, and M. L. Myrick, Appl. Spectrosc. **50,** 552 (1996).
5. P. A. Mosier–Boss, S. H. Lieberman, and R. Newbery, Appl. Spectrosc. **49,** 630 (1995).
6. D. Zhang and D. Ben–Amotz, Appl. Spectrosc. **54,** 1379 (2000).
7. A. Savitzky and M. J. E. Golay, Anal. Chem. **36,** 1627 (1964).
8. X. Shao and W. Cai, Rev. Anal. Chem. **17,** 235 (1998).
9. F. T. Chau, J. B. Gao, T. M. Shih, and J. Wang, Appl. Spectrosc. **51,** 649 (1997).
10. X. Shao, H. Zhong, M. Zhang, and G. Zhao, Spectroscopy and Spectral Analysis **17,** 85 (1997).
11. V. J. Barclay, R. F. Bonner, and I. P. Hamilton, Anal. Chem. **69,** 78 (1997).
12. M. Bos and J. A. M. Vrielink, Chemom. Intell. Lab. Syst. **23,** 115 (1994).
13. U. Depczynski, K. Jetter, K. Molt, and A. Miemoller, Chemom. Intell. Lab. Syst. **47,** 179 (1999).
14. L. L. Biehl and D. A. Langrebe, presented at Pecora 13, Sioux Falls, South Dakota (1996), http://dynamo.ecn.purdue.edu/biehl/multi.spec.
15. S. Mallat, IEEE Trans. on Patt. Anal. Machine. Intell. **11,** 674 (1989).
16. I. Daubechies, *Ten Lectures on Wavelets* (AIAM, Philadelphia, 1992).
17. Y. Meyer, *Wavelets and Operators* (Cambridge University Press, Cambridge, 1992).
18. D. L. Donoho and I. M. Johnstone, Biometrika **81,** 425 (1994).
19. T. Cai, Ann. Statist. **27,** 898 (1999).
20. A. D. Gift, Y. Ma, K. S. Haber, B. L. Maclain, and D. Ben–Amotz, J. Raman Spectrosc. **30,** 757 (1999).